

Chern numbers for the index surfaces of photonic crystals: conical refraction as a basis for topological materials

R. L. Mc Guinness and P. R. Eastham

School of Physics and CRANN, Trinity College Dublin, Dublin 2, Ireland.

(Dated: September 14, 2020)

The classification of bandstructures by topological invariants provides a powerful tool for understanding phenomena such as the quantum Hall effect. This classification was originally developed in the context of electrons, but can also be applied to photonic crystals. In this paper we study the topological classification of the refractive index surfaces of two-dimensional photonic crystals. We consider crystals formed from birefringent materials, in which the constitutive relation provides an optical spin-orbit coupling. We show that this coupling, in conjunction with optical activity, can lead to a gapped set of index surfaces with non-zero Chern numbers. This method for designing photonic Chern insulators exploits birefringence rather than lattice structure, and does not require band crossings originating from specific lattice geometries.

I. INTRODUCTION

Chern insulators are two-dimensional materials that are insulating in their interior but conducting along their edge. The first such materials to be identified were the integer quantum Hall states [1], for which the quantized Hall conductance corresponds to a topological invariant known as the Chern number [2–4]. The Chern number is related to the number of conductive edge states at the interface between a topologically non-trivial insulator and a topologically trivial one [5]. A later example of a Chern insulator is provided by the Haldane model [6], which introduced a now well-trodden path to constructing topologically non-trivial bandstructures. This model describes particles hopping on a two-dimensional hexagonal lattice, an arrangement which produces point degeneracies in the bandstructure. These are the celebrated Dirac points, which are associated with vortex-like singularities in the Bloch functions. They can be a precursor to a topologically non-trivial gapped bandstructure, which arises if the degeneracies are split by a perturbation in such a way that the windings of the vortices combine rather than cancel [7].

Topologically non-trivial bandstructures are not restricted to theories of electrons, but can also be achieved for photons [8–18], polaritons [19–22], and sound waves [23–25]. The possibility of topological photonic bands was raised by Haldane and Raghu [8, 9], who showed how the original Haldane model could be implemented for light in a hexagonal photonic crystal. Many subsequent works have followed this proposal, showing how the degeneracies of photonic lattices can be split to achieve either a Z photonic Chern insulator [9, 10, 13] or a Z_2 photonic topological insulator [15, 16]. Often such works consider situations where the polarization and propagation decouple as, for example, for the TE and TM modes propagating in the plane of a 2D photonic crystal. However, such decoupling does not occur in an optically anisotropic material or structure, where the polarization states depend on the wavevector direction.

The topological classification of photonic materials is

usually based on their dispersion relation, i.e., the bandstructure, and the associated Bloch states. Another important quantity, however, is the refractive index surface. This is related to, but distinct from, the dispersion relation: it is the surface of wavevectors corresponding to a particular frequency. In this paper we study topological effects that derive from the refractive index surface. We show how the generic features of the index surfaces of anisotropic bulk materials lead, in periodic systems based on such materials, to a type of photonic Chern insulator.

Our focus is on two-dimensional photonic crystals formed from biaxial materials or metamaterials. For such materials the index surface consists of two ellipsoids that intersect at conical singularities, which are point degeneracies that are equivalent to the Dirac points of a dispersion relation. In a periodic system the index surface consists of many sheets defined on a two-dimensional Brillouin zone, and contains conical intersections inherited from those of the bulk, as shown in Fig. 1. These can be split in such a way as to achieve a gapped set of index surfaces with non-zero Chern numbers, i.e., a form of optical Chern insulator. Our approach is based on effective medium theory, and exploits the singularities that are generic, topologically enforced features of optical index surfaces, rather than those of particular lattices. This suggests that similar Chern index surfaces could be achieved in two-dimensional photonic structures with a range of lattice geometries.

A related concept of photonic Chern insulators has been put forward by Gao et al. [26]. That work, however, considers an optically homogeneous material, for which the refractive index is defined on the sphere of wavevector directions. We consider instead a periodic material, and specifically a two-dimensional photonic crystal. In this case the refractive index is defined not on a sphere, but on a two-dimensional torus, i.e. the Brillouin zone. This change in the underlying topology necessitates a different approach to designing topological materials. We note also that the topological classification of the index surface of a periodic structure is implicit in the tight-binding model of the photonic Floquet topological insulator, as realized on a hexagonal lattice [13]. The present work

places this type of state within the broader context of the optics of periodic anisotropic materials, and reveals a different approach to its realization.

II. MODEL

We consider the propagation of light, at some fixed frequency ω , through a two-dimensional photonic crystal, and seek to map this problem to a Schrodinger equation with a topologically non-trivial Hamiltonian. We do this via the refractive index surface, which is a polar plot of the refractive index n over all possible wavevector directions. Since $n = ck/\omega$, where k is the magnitude of the wavevector, the index surface is a constant-frequency surface in wavevector space, akin to the Fermi surface of a solid. The connection to a Schrodinger equation follows on noting that the index surface determines one wavevector component (propagation constant) in terms of the other two, $k_z = \sqrt{n^2\omega^2/c^2 - k_x^2 - k_y^2}$, so for a scalar field we have $i\partial_z\psi(k_x, k_y, z) = k_z\psi(k_x, k_y, z) \equiv H\psi(k_x, k_y, z)$. The polarization of light may be included by replacing ψ with a two-component field, formed from the complex amplitudes of two orthogonal polarization states. In an anisotropic material there will be two distinct refractive indices n_{\pm} for each wavevector direction, each associated with a particular, wavevector-dependent polarization. Thus H becomes an operator acting in both spin (polarization) space and real space, with spin-orbit coupling terms [27].

The forms of index surface for various dielectrics are well known [28, 29]. We consider here the most general case of a biaxial material. For such materials the dielectric tensor possesses three distinct eigenvalues $\epsilon_1 \neq \epsilon_2 \neq \epsilon_3$, and the index surface consists of two ellipsoids. These ellipsoids intersect at four conical singularities, one of which is shown in Fig. 1a. The wavevectors of these singularities are the optic axes of the crystal, along which light undergoes conical refraction [30]. Near a singularity the effective Hamiltonian, in the basis of circular polarization states, takes the Dirac-point form $H = A\hat{\sigma}\cdot(k_x, k_y, 0)$, where k_x, k_y are components of the wavevector perpendicular to the optic axis [27]. The quantity A , which plays the role of the Fermi velocity, is the semi-angle of the conical intersection. If we introduce a periodic modulation in a plane containing the wavevectors k_x and k_y then they become defined on a two-dimensional Brillouin zone, and additional singularities appear in the index surface (Fig. 1c). Optical activity splits these singularities (Figs. 1b, 1d) and, as we show in the following, this can be done in such a way as to achieve a non-zero Chern number.

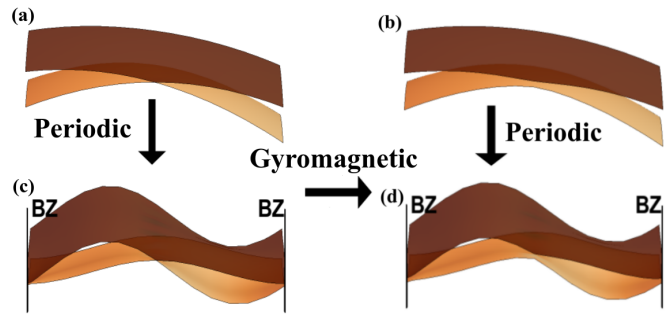


FIG. 1. (Color online) Illustration of the formation of topologically non-trivial index surfaces in two-dimensional photonic crystals. Each panel is a schematic of a section of a refractive index (isofrequency) surface, for (a) a biaxial dielectric, (b) a biaxial dielectric with optical activity, (c) a periodic biaxial dielectric, (d) a periodic biaxial dielectric with optical activity. Each panel is centered on the wavevector corresponding to the conical singularity in (a). The periodicity is taken to be in the plane perpendicular to this wavevector, forming a two-dimensional Brillouin zone (BZ).

A. Effective Hamiltonian: paraxial approximation

To demonstrate the formation of non-zero Chern numbers for the index surface we will consider the specific case of a two-dimensional photonic crystal, with periodicity perpendicular to an optic axis. We will develop an effective Hamiltonian based on the paraxial approximation to the index surface of a homogeneous dielectric. As discussed in Refs. 27, 30–33, considering plane-wave solutions to Maxwell's equations in such a dielectric leads to an eigenvalue problem

$$Md_{\pm} = \lambda d_{\pm} = d_{\pm}/n_{\pm}^2, \quad (1)$$

where the two-dimensional matrix M depends on the propagation direction $\hat{\mathbf{k}}$ and the dielectric tensor. For each direction there are two distinct refractive indices n_{\pm} , and two corresponding polarization states. Each of the latter is specified by the two-component complex vectors d_{\pm} for which we use the basis of circular polarizations.

As discussed above, Eq. (1) corresponds to a two-dimensional Hamiltonian for propagating the field forwards in z ; this Hamiltonian is a matrix whose eigenvalues are $k_{z,\pm}(k_x, k_y)$, and whose eigenvectors are $d_{\pm}(k_x, k_y)$. Since the behavior of the homogeneous dielectric is scale-invariant we may introduce the characteristic wavevector $k_0 = \omega/c$ and write $i\partial_z\psi = k_0H\psi$, where H is the matrix whose eigenvalues are $\sqrt{n_{\pm}^2 - \tilde{k}_x^2 - \tilde{k}_y^2}$, where $\tilde{k}_x = k_x/k_0$. We now specialize to consider wavevectors which are close to the z direction. Thus $\tilde{k}_x, \tilde{k}_y \ll 1$ and we may expand H as a power series in these quantities. This leads to a paraxial approximation

$$H_p = h_0(\tilde{k}_x, \tilde{k}_y)I + \mathbf{h}(\tilde{k}_x, \tilde{k}_y)\cdot\hat{\sigma}, \quad (2)$$

where h_0 and \mathbf{h} are second-order polynomials in the off-axis components of wave vector. The forms of these polynomials are given in the appendix, for the case of propagation near to an optic axis in a material with biaxiality and anisotropic optical activity.

The paraxial Hamiltonian H_p gives a local approximation to the index surfaces near the propagation direction, taken to lie along the optic axis. This local approximation should give a reasonable account of the topological structure of the index surface so long as the range of transverse wavevectors does not encompass any other singularities. The part of the Hamiltonian proportional to h_0 controls the overall curvature of the index surfaces. In the absence of optical activity, the index surface is split into two linearly-polarized surfaces due to the off-diagonal components proportional to h_x and h_y , which vanish at the optic axis. Optical activity lifts the degeneracy of the two circular polarizations at these points, and the index surfaces are gapped everywhere. As we shall see, a non-zero Chern number in the periodic case requires an anisotropic optical activity. For definiteness we suppose this to arise from the Faraday effect, which is parameterized by an optical activity vector \mathbf{g} that is related to the applied field (see appendix).

B. Periodic generalization

The Chern numbers of a bandstructure are integer topological invariants, which characterize the mapping between the closed two-dimensional Brillouin zone and the states defined by the Hamiltonian [2, 4]. The states for each band $|\psi(k_x, k_y)\rangle$ provide a $U(1)$ Berry connection $A_i = i\langle\psi|\partial_{k_i}|\psi\rangle$ and flux $F = \partial_x A_y - \partial_y A_x$, whose integral over the Brillouin zone is 2π times the Chern number of the band [34]. The Hamiltonian H_p discussed above, however, does not define a quantized Chern number, because it is defined on an open disk of wavevectors $k_x^2 + k_y^2 < n_-^2 k_0^2$ rather than a closed, two-dimensional Brillouin zone. We must therefore generalize it so as to apply to a periodic structure.

In order to do this we will consider the lattice version of the Hamiltonian H_p , for simplicity considering a square lattice in the $x - y$ plane with lattice constant a . The real-space lattice Hamiltonian is obtained from H_p by replacing the derivatives, $k_i = -i\partial_i$, with finite differences. In wavevector space this corresponds to making the replacements

$$\begin{aligned} k_i &\rightarrow \frac{1}{a} \sin k_i a \\ k_i^2 &\rightarrow \frac{2}{a^2} [1 - \cos k_i a], \end{aligned} \quad (3)$$

giving the wavevectors, and hence the Hamiltonian, the appropriate periodicity. As we shall see, this periodic Hamiltonian gives a qualitative description of the topological features of the index surfaces obtained from plane-wave calculations. It is equivalent to a tight-binding

model at a particular choice of hopping parameters. We shall denote it by H_l and introduce the wavevector scale in the material $k = \sqrt{\epsilon_2} k_0$ for later convenience.

The effect of introducing periodicity is illustrated in Fig. 1, which shows the evolution of the index surfaces of a homogeneous biaxial material as optical activity, periodicity, or both are added. The key feature of the reformulated Hamiltonian H_l is that, in the absence of optical activity, there are additional degeneracies in the first Brillouin zone. This is a consequence of the periodic topology of the Brillouin zone, which requires the vector field ($h_x, h_y, h_z = 0$) to have zero net circulation. We shall now move to classifying the topological character of the index surfaces of these photonic crystals.

III. RESULTS

A. Topological phases of the lattice model

The topological phases of the lattice model can be deduced from the degeneracy structure of the Hamiltonian H_l [7]. For a two-band Hamiltonian such as H_l the Chern number, C , is the winding number of the vector field $\mathbf{h}(k_x, k_y)$. It can be computed by summing over the zeros of (h_x, h_y) in the Brillouin zone

$$C = \sum_i v_i \text{sgn } h_z(i), \quad (4)$$

where i denotes a zero of (h_x, h_y) in the Brillouin zone, at which the vorticity is v_i and the mass term $h_z(i)$.

We therefore discuss first the case of zero magnetic field, so that $h_z = 0$. Fig. 2 shows the field $(h_x, h_y) = |h|(\cos 2\theta, \sin 2\theta)$, along with the zero contour lines of these components. This field shows the direction of linear polarization θ for the outermost sheet of the index surface. The intersections of the contour lines are the conical singularities or Dirac points, where the sheets of the index surface are degenerate. For illustration we take the permittivities $\epsilon_1 = 2.25$, $\epsilon_2 = 2.5$, $\epsilon_3 = 2.75$ and a lattice spacing to wavelength ratio of $a/\lambda = 4/5$. We use these permittivities for the remainder of this paper, and this lattice spacing to wavelength ratio except where otherwise stated.

As can be seen in Fig. 2, the lattice periodicity has introduced additional conical singularities in the index surfaces. These are at the intersections of the zero contour lines of h_x (turquoise) and h_y (green), and for these parameters there are two such intersections in the first Brillouin zone. In addition to the Dirac point at Γ , corresponding to that of the original index surface, there is a second Dirac point just inside the X boundary along the line $k_y = 0$. The Berry flux corresponding to each of these singularities is $\pm\pi$, so that with two degeneracies in the first Brillouin zone we can achieve a Chern number $C \in \{-1, 0, 1\}$.

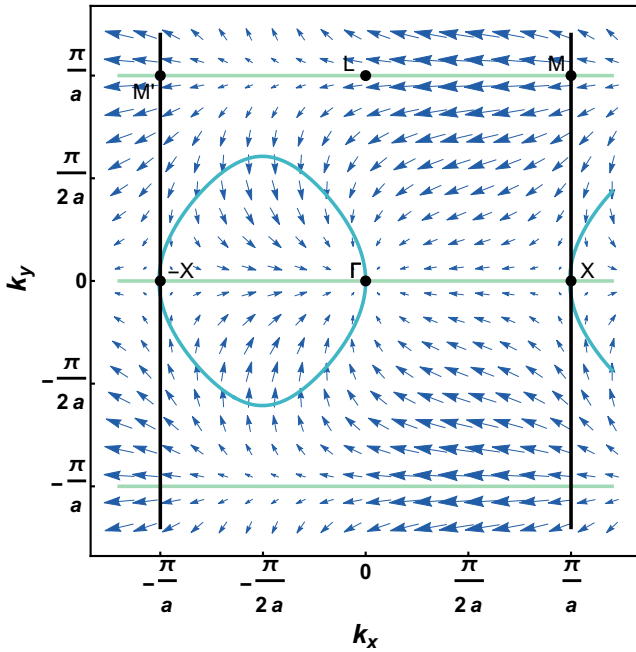


FIG. 2. (Color online) Polarization structure of the index surface over the first Brillouin zone for a biaxial material and a square lattice, predicted by Eqs. (2) and (3). The arrows show the field $(\mathbf{h}_x; \mathbf{h}_y)$. The zeros of \mathbf{h}_x and \mathbf{h}_y lie along the lines indicated in turquoise (dark grey) and green (light grey), respectively. In the absence of optical activity $\mathbf{h}_z = 0$ and there are conical singularities at the intersections of the contours shown. The first Brillouin zone is the square bounded by the two black lines and the upper and lower green contours. The parameters are $\alpha_1 = 2:25$, $\alpha_2 = 2:5$, $\alpha_3 = 2:75$ and $ka = 1:6$, where $\mathbf{k} = |\mathbf{k}|(\mathbf{c}\sqrt{2})$.

Optical activity due to the Faraday effect introduces a term $h_z \neq 0$ and lifts the degeneracies in the index surface. The polarization over the index surface then becomes elliptical, with a circularity determined by the sign of h_z . To achieve a non-zero Chern number the zero contour of $h_z(k_x, k_y)$ must separate the two lifted degeneracies, so that h_z has opposite signs at each of them, and the signs of their Berry fluxes are the same [Eq. (4)]. Physically, the circular polarization must swap between the two C-points in each sheet around which the linear polarization winds. Whether or not this occurs depends on the direction of the optical activity vector.

In Figure 3 we show how the Chern number depends on the direction of the optical activity vector. It shows the Chern number by shading for a range of directions (θ, ϕ) about and around the equator $\theta = \frac{\pi}{2}$ at which the field and optic axis are perpendicular. We see that non-zero Chern numbers (light and dark shading) can be achieved, for this model, when the optical activity vector lies almost perpendicular to the optic axis. This region is bounded by two equators: one perpendicular to the optic axis, which corresponds to gap closing at the Γ point, and one at a slightly different angle, which corresponds to the gap closing at the C-point near to

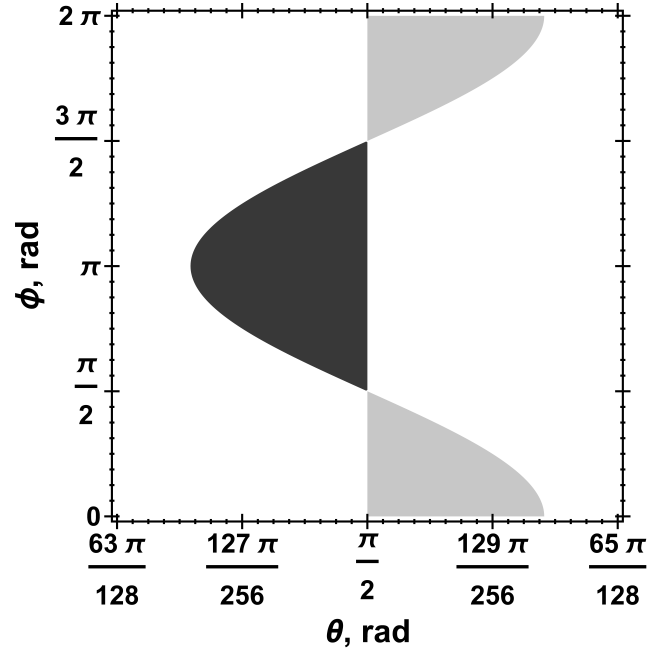


FIG. 3. Chern number \mathbf{C} (shading) of a biaxial material on a square lattice, from the paraxial Hamiltonian model, with optical activity due to the Faraday effect. The spherical coordinates $(\theta; \phi)$ give the direction of the axis of optical activity, i.e. the magnetic field. The polar angle ϕ is measured from the optic axis, and the azimuthal angle θ from the x-axis of the rotated coordinate system described in the appendix. The shadings represent $\mathbf{C} = 0$ (white) and $\mathbf{C} = \pm 1$ (dark/light grey). The parameters are those given in Fig. 2.

X. The existence of a finite region between these two equators, where the Chern number is non-zero, is due, primarily, to the displacement of this latter C-point from the zone boundary.

The phase diagram in Figure 3 does not depend on the strength of the optical activity, although of course this parameter does affect the size of the gap. The dependence we have observed on the remaining parameters of the model is related to the displacement of the C-point away from the zone boundary. In the model H_I this displacement arises from the interplay of the linear and quadratic terms in the paraxial Hamiltonian, which give different contributions to the lattice model that vanish at different points in the zone [see Eq. (3)]. If we increase the cone angle A , i.e. the degree of biaxiality, the C-point near X moves into the Brillouin zone along the $k_y = 0$ line, and the region of non-zero Chern number in Fig. 3 expands. We can also vary the ratio of the lattice spacing to the operating wavelength, ka , which controls the paraxial approximation, Eq. (2). As this parameter increases the second-order terms decrease relative to the first-order ones, bringing the C-point near X closer to the zone boundary, and reducing the region of non-zero Chern number.

B. Simulated index surfaces

In this subsection we compare the periodic Hamiltonian model, H_I , to the index surfaces extracted from a plane-wave calculation of a two-dimensional photonic crystal [35]. We focus on the locations of the singularities in a material without optical activity, since this is the key feature determining the topological phase diagram when optical activity is introduced. We consider specifically a biaxial dielectric in which cylindrical air holes are drilled to form a square lattice.

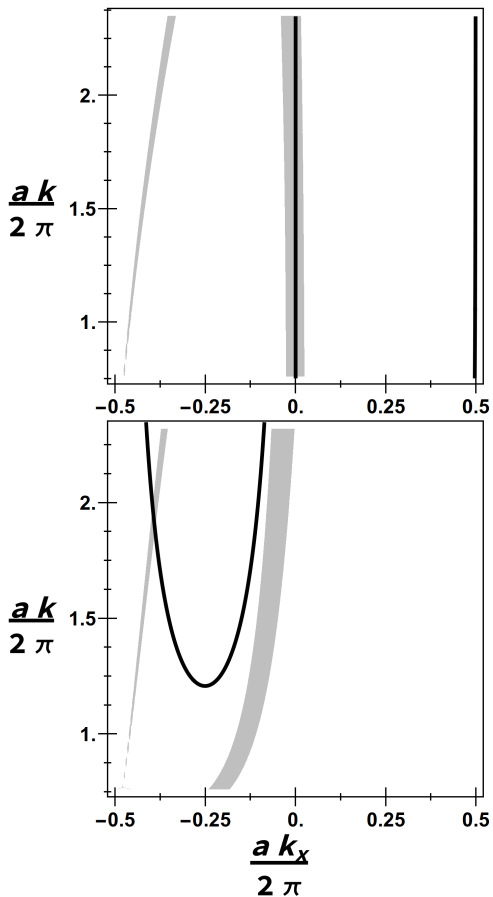


FIG. 4. Comparison of the locations of the Dirac points given by the paraxial theory and a frequency-domain plane-wave simulation as \mathbf{k} is varied. In both cases Dirac points occur along the lines $k_y = 0$ (top) and $k_y = \pi/a$ (bottom). Solid lines: k_x for the Dirac points from the paraxial theory. Shading: bounds on k_x for the Dirac points from the plane-wave simulations, where the magnitude of the splitting between the index surfaces is smaller than $a\Delta k_z = 2 \times 10^{-6}$. The dielectric parameters are those in Fig. 2. The plane-wave simulation has cylindrical air holes in the dielectric background, with a filling factor of $(0.15)^2$.

In Fig. 4 we compare how the locations of the Dirac points evolve with the wavevector scale k , at fixed a , in the two theories. The solid black lines show the locations predicted by H_I , while those predicted numerically lie within the shaded regions of the figure. We see that H_I

gives a reasonable account of the numerical results. As shown in the upper panel, it correctly predicts the two Dirac points along the line $k_y = 0$ for all values of ka , i.e., for all degrees of paraxiality. As expected there is a Dirac point along $k_y = 0$ at $k_x = 0$ in both theories. There is also a second Dirac point present in each theory along this line. For the periodic Hamiltonian model the second Dirac point is adjacent to the positive k_x Brillouin zone boundary; for the the numerical simulations the Dirac point is found on the other side of this boundary displaced from the zone edge. We attribute this difference to the different treatment of scattering in the two methods, and perhaps also to higher-order terms neglected in Eq. (2). The lower panel of Fig. 4 shows the positions of Dirac points along the line $k_y = \pi/a$. While for small ka the model H_I lacks the two Dirac points seen in the numerical simulation, there is a critical ka above which this additional pair emerges. Above this critical ka the model H_I is in qualitative agreement with the numerical simulation.

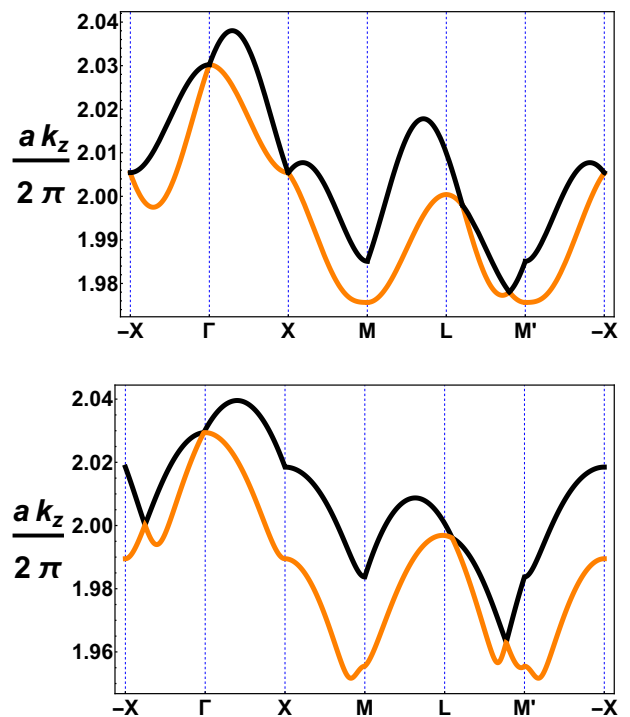


FIG. 5. (Color online) Index surfaces along high-symmetry directions of the first Brillouin zone from the paraxial model (top panel) and a frequency-domain plane-wave calculation (lower panel). The relevant high-symmetry points are indicated in Fig. 2. $ka \simeq 4$, and all other parameters are as in Figs. 2 and 4.

In Figure 5 we compare the index surfaces of the two theories, along a high-symmetry path through the Brillouin zone, for $ka \simeq 4\pi$. This degree of paraxiality places us in a regime towards the top of the vertical scale of the plots in Figure 4, in which there are four Dirac points in

the Brillouin zone. As can be seen in this figure, there is a reasonable correspondence between the forms of the index surfaces of the two theories. As expected the shapes of the bands are somewhat different. Nonetheless, given the correspondence between the numbers and locations of the Dirac points across most degrees of paraxiality, the topological phase diagrams of the two models will be similar to one another. In the regime before the additional Dirac points emerge in the model H_l the phase diagram of the numerical simulation will be richer than that of the model.

IV. DISCUSSION

In this paper we have explored the refractive index surfaces of two-dimensional photonic crystals. We have shown how optical activity can lead to photonic materials characterized by gapped, i.e. non-degenerate, index surfaces with non-zero Chern numbers. Our approach is unusual in that it does not rely on a specific lattice geometry, but instead on the conical intersections that occur generically in the index surface of optically anisotropic materials. This suggests that such topological photonic materials can be constructed with a range of lattice geometries.

For brevity we have referred to our material as a photonic Chern insulator. However, as can be seen from Fig. 5, it generally lacks a band gap at a particular propagation constant, and so is more accurately described as a photonic semi-metal with topological bands. In a true Chern insulator the topology of the bulk bands leads, in the presence of an interface, to the appearance of edge-states in the gap. For the semi-metal one does expect that a slow spatial variation of the structure from one topological phase to another will introduce modes crossing the bulk bands. However, a generic realistic interface would allow these modes to mix with the bulk bands and destroy their localization. Given that our proposal is not dependent on the particular form of lattice geometry, however, it should be possible to adapt the lattice to achieve a true Chern insulator. Furthermore, although one does not necessarily expect conventional edge states, topological semi-metals are known to have interesting properties in their own right [36].

ACKNOWLEDGMENTS

We acknowledge support from the Irish Research Council award GOIPG/2015/3570 and Science Foundation Ireland award 15/IACA/3402.

Appendix: Paraxial Hamiltonian

In this appendix we give the forms of the paraxial Hamiltonian H_p for propagation close to the optic axis, in

materials with biaxiality and anisotropic optical activity. They extend the results in Ref. 33 to include all terms up to second-order in the off-axis wavevectors, which is necessary to achieve a non-trivial topology for the periodic form of H_p . These expressions are obtained by rotating the spatial coordinates so that z lies along an optic axis, expanding the expressions for $k_{z,\pm}$ to construct a diagonalized form for the paraxial Hamiltonian in the eigenbasis of M , and transforming the result out of this eigenbasis. For comparison with Ref. 37 we use the scaled transverse wavevectors $p_{x,y} = k_{x,y}/k = \tilde{k}_{x,y}/\sqrt{\epsilon_2}$, where $k = k_0\sqrt{\epsilon_2} = \omega\sqrt{\epsilon_2}/c$ is the wavevector at frequency ω in an isotropic material of permittivity ϵ_2 . Note however that we use a circular polarization basis rather than the linear one of Ref. 37.

Considering first a biaxial dielectric without optical activity, characterized by principal dielectric constants $\epsilon_1 < \epsilon_2 < \epsilon_3$, we find

$$\begin{aligned} h_{0,B} &= -Ap_x + \frac{1}{4}[2 + \epsilon_2(\alpha - \beta) - 12A^2]p_x^2 + \\ &\quad + \frac{1}{4}[2 + \epsilon_2(\alpha - \beta) - 6A^2]p_y^2. \\ h_{x,B} &= -Ap_x + \frac{1}{4}[\epsilon_2(\alpha - \beta) - 12A^2]p_x^2 \\ &\quad - \frac{1}{4}\epsilon_2(\alpha + 3\beta)p_y^2, \\ h_{y,B} &= -Ap_y + \frac{1}{2}[\epsilon_2(\alpha + \beta) - 6A^2]p_x p_y. \\ h_{z,B} &= 0. \end{aligned} \tag{A.1}$$

Here $\alpha = \epsilon_1^{-1} - \epsilon_2^{-1}$ and $\beta = \epsilon_2^{-1} - \epsilon_3^{-1}$ are measures of the spread of the principal dielectric constants of the biaxial material and A is the biaxial cone semi-angle, defined as $A = \frac{1}{2}\epsilon_2\sqrt{\alpha\beta}$. Sufficiently close to the optic axis direction this Hamiltonian takes a Dirac point form.

Optical activity introduces an antisymmetric contribution to the inverse of the relative permittivity tensor $\eta_{ik} = (\epsilon^{-1})_{ik}$, corresponding to a contribution $\epsilon_0 \mathbf{E} = i\mathbf{D} \times \mathbf{g}$ in the constitutive relation, where \mathbf{g} is the optical activity vector [29, 31]. In the case of the Faraday effect the optical activity vector is proportional to the applied field, $g_i = \gamma_{ij}H_j$, and independent of the wavevector. In the paraxial Hamiltonian this introduces additional terms in h_0 , describing the field's effect on the overall dispersion relation, as well as terms in h_3 , describing the anisotropic splitting between the circular polarization states. The expressions for these components are

$$\begin{aligned} h_{0,F} &= h_{0,B} - \frac{3}{8}\epsilon_2^2[g_3'^2 + 2g_3'(g_1' p_x + g_2' p_y) + \\ &\quad + (g_1'^2 - g_3'^2)p_x^2 + 2g_1'g_2' p_x p_y + (g_2'^2 - g_3'^2)p_y^2]. \end{aligned} \tag{A.2}$$

and

$$\begin{aligned}
h_{z,F} = \frac{1}{2}\epsilon_2 \left(g'_3 + (g'_1 + 3Ag'_3)p_x + g'_2p_y \right. \\
\left. - \frac{1}{2}\{g'_3[1 + \frac{3}{2}\epsilon_2(\alpha - \beta)] - 6Ag'_1\}p_x^2 \right. \\
\left. + 3Ag'_2p_xp_y - \frac{1}{2}\{g'_3[1 + \frac{3}{2}\epsilon_2(\alpha - \beta)]\}p_y^2 \right). \tag{A.3}
\end{aligned}$$

Here \mathbf{g}' is the optical activity vector in the rotated basis, where z lies along the optic axis. The relation to the optical activity vector in the principal axes coordinate system (where ϵ is diagonal) is $\mathbf{g}' = R\mathbf{g}$ with

$$R = \begin{pmatrix} \sqrt{\frac{\beta}{\alpha+\beta}} & 0 & -\sqrt{\frac{\alpha}{\alpha+\beta}} \\ 0 & 1 & 0 \\ \sqrt{\frac{\alpha}{\alpha+\beta}} & 0 & \sqrt{\frac{\beta}{\alpha+\beta}} \end{pmatrix}. \tag{A.4}$$

For completeness we note that, in the case of a chiral medium, the optical activity vector is related to the wavevector direction, $g_i = \Gamma_{ij}k_j$, by a symmetric tensor

Γ_{ij} [29, 37]. This modifies the components h_0 and h_3 as follows:

$$\begin{aligned}
h_{0,C} = h_{0,B} - \frac{3}{8}\epsilon_2^2 \{ \Gamma_{33}'^2 + 4\Gamma_{13}'\Gamma_{33}'p_x + 4\Gamma_{23}'\Gamma_{33}'p_y + \\
+ [4\Gamma_{13}'^2 + 2\Gamma_{33}'(\Gamma_{11}' - \Gamma_{33}')]p_x^2 + \\
+ 4(\Gamma_{12}'\Gamma_{33}' + 2\Gamma_{13}'\Gamma_{23}')p_xp_y + \\
+ [4\Gamma_{23}'^2 + 2\Gamma_{33}'(\Gamma_{22}' - \Gamma_{33}')]p_y^2 \}. \tag{A.5}
\end{aligned}$$

and

$$\begin{aligned}
h_{z,C} = \frac{1}{2}\epsilon_2 \left(\Gamma_{33}' + (2\Gamma_{13}' + 3A\Gamma_{33}')p_x + 2\Gamma_{23}'p_y \right. \\
\left. + \{\Gamma_{11}' + 6A\Gamma_{13}' - [1 + \frac{3}{4}\epsilon_2(\alpha - \beta)]\Gamma_{33}'\}p_x^2 \right. \\
\left. + (2\Gamma_{12}' + 6A\Gamma_{23}')p_xp_y \right. \\
\left. + \{\Gamma_{22}' - [1 + \frac{3}{4}\epsilon_2(\alpha - \beta)]\Gamma_{33}'\}p_y^2 \right). \tag{A.6}
\end{aligned}$$

where the tensor Γ' is related to the corresponding tensor in the principal axes basis by $\Gamma' = R\Gamma R^{-1}$.

-
- [1] K. v. Klitzing, G. Dorda, and M. Pepper, Phys. Rev. Lett. **45**, 494 (1980).
- [2] J. E. Avron, R. Seiler, and B. Simon, Phys. Rev. Lett. **51**, 51 (1983).
- [3] M. Kohmoto, Ann. Phys. (NY) **160**, 343 (1985).
- [4] D. J. Thouless, M. Kohmoto, M. P. Nightingale, and M. den Nijs, Phys. Rev. Lett. **49**, 405 (1982).
- [5] Y. Hatsugai, Phys. Rev. Lett. **71**, 3697 (1993).
- [6] F. D. M. Haldane, Phys. Rev. Lett. **61**, 2015 (1988).
- [7] D. Sticlet, F. Piéchon, J.-N. Fuchs, P. Kalugin, and P. Simon, Phys. Rev. B **85**, 165456 (2012).
- [8] S. Raghu and F. D. M. Haldane, Phys. Rev. A **78**, 033834 (2008).
- [9] F. D. M. Haldane and S. Raghu, Phys. Rev. Lett. **100**, 013904 (2008).
- [10] T. Ochiai and M. Onoda, Phys. Rev. B **80**, 155103 (2009).
- [11] Z. Wang, Y. D. Chong, J. D. Joannopoulos, and M. Soljačić, Phys. Rev. Lett. **100**, 013905 (2008).
- [12] Z. Wang, Y. Chong, J. D. Joannopoulos, and M. Soljačić, Nature **461**, 772 (2009).
- [13] M. C. Rechtsman, J. M. Zeuner, Y. Plotnik, Y. Lumer, D. Podolsky, F. Dreisow, S. Nolte, M. Segev, and A. Szameit, Nature **496**, 196 (2013).
- [14] Y. Poo, R.-x. Wu, Z. Lin, Y. Yang, and C. T. Chan, Phys. Rev. Lett. **106**, 093903 (2011).
- [15] A. B. Khanikaev, S. Hossein Mousavi, W.-K. Tse, M. Kargarian, A. H. MacDonald, and G. Shvets, Nat Mater **12**, 233 (2013).
- [16] W.-J. Chen, S.-J. Jiang, X.-D. Chen, B. Zhu, L. Zhou, J.-W. Dong, and C. T. Chan, Nat. Commun. **5**, 5782 (2014).
- [17] T. Ma, A. B. Khanikaev, S. H. Mousavi, and G. Shvets, Phys. Rev. Lett. **114**, 127401 (2015).
- [18] A. Slobozhanyuk, H. S. Mousavi, X. Ni, D. Smirnova, Y. S. Kivshar, and A. B. Khanikaev, Nat. Photon **11**, 130 (2017).
- [19] C.-E. Bardyn, T. Karzig, G. Refael, and T. C. H. Liew, Phys. Rev. B **91**, 161413 (2015).
- [20] A. V. Nalitov, D. D. Solnyshkov, and G. Malpuech, Phys. Rev. Lett. **114**, 116401 (2015).
- [21] T. Karzig, C.-E. Bardyn, N. H. Lindner, and G. Refael, Phys. Rev. X **5**, 031001 (2015).
- [22] K. Yi and T. Karzig, Phys. Rev. B **93**, 104303 (2016).
- [23] E. Prodan and C. Prodan, Phys. Rev. Lett. **103**, 248101 (2009).
- [24] C. L. Kane and T. C. Lubensky, Nat. Phys. **10**, 39 (2014).
- [25] Z. Yang, F. Gao, X. Shi, X. Lin, Z. Gao, Y. Chong, and B. Zhang, Phys. Rev. Lett. **114**, 114301 (2015).
- [26] W. Gao, M. Lawrence, B. Yang, F. Liu, F. Fang, B. Béri, J. Li, and S. Zhang, Phys. Rev. Lett. **114**, 037402 (2015).
- [27] M. V. Berry and M. R. Jeffrey, J. Opt. A **8**, 363 (2006).
- [28] M. Born and E. Wolf, *Principles of Optics*, 7th ed. (CUP, 1999).
- [29] L. D. Landau, E. M. Lifshitz, and L. P. Pitaevskii, *Electrodynamics of continuous media*, 2nd ed., Course of theoretical physics (Elsevier, Butterworth-Heinemann, Amsterdam, 2008).
- [30] M. Berry, M. Jeffrey, and J. Lunney, Proc. Royal Soc. Lond. A **462**, 1629 (2006).
- [31] M. V. Berry and M. R. Dennis, Proc. Royal Soc. Lond. A **459**, 1261 (2003).
- [32] M. V. Berry, J. Opt. A **6**, 289 (2004).
- [33] M. Jeffrey, *Conical Diffraction: Complexifying Hamil-*

- tons Diabolical Legacy*, Ph.D. thesis, University of Bristol (2007).
- [34] T. Fukui, Y. Hatsugai, and H. Suzuki, *J. Phys. Soc. Jpn.* **74**, 1674 (2005).
- [35] S. G. Johnson and J. D. Joannopoulos, *Opt. Express* **8**, 173 (2001).
- [36] A. Burkov, *Nat. Mater.* **15**, 1145 (2016).
- [37] M. V. Berry, M. R. Jeffrey, and M. Mansuripur, *J. Opt. A* **7**, 685 (2005).